This article has been accepted for publication in a future issue of this journal, but has not been fully edited. Content may change prior to final publication. Citation information: DOI 10.1109/JSEN.2018.2867208, IEEE Sensors Journal

Design and Experimentation of a Batteryless On-skin RFID Graphene-Oxide Sensor for the Monitoring and Discrimination of Breath Anomalies

M. C. Caccami, M. Y. S. Mulla, C. Occhiuzzi, C. Di Natale, and G. Marrocco

***Abstract*—Real-time and comfortable monitoring of the human breathing could allow identifying anomalies in the rhythm and waveform to be correlated with several pathologic disorders of respiratory and cardiovascular systems. A wireless sensor based on a flexible kapton substrate, suitable to be stuck over the face skin like a plaster and provided with a graphene-oxide (GO) electrode, is here proposed for application to the monitoring of the moisture emitted during inhalations and exhalations. The GO-based electrode increases its DC resistance when exposed to humidity with a sensitivity of 60 Ω/RH. The device is compatible with the Radiofrequency Identification (RFID) standard in the UHF band. When used in battery-less mode it can be read up to 60 cm. The RFID sensor has been successfully experimented in a measurement campaign involving ten volunteers asked to reproduce a set of predefined normal and pathological breaths. The resulting resistance traces permit to well clusterize the breath patterns with respect to the respiration rate (extracted by an FFT) and to the average peak variation of the sensor's resistance with an accuracy close to 90%.**

***Index Terms*—Breath sensor, graphene oxide, RFID technology, skin antenna, wireless monitoring**

I. Introduction[1]

Breathing is a rhythmic physiological act that occurs unconsciously and guarantees the supply of oxygen for human survival [1]. Anomalies in respiration rate and the tidal volume variability can be correlated with disorders of the cardiovascular system as well as with the obstructive sleep apnea syndrome (OSA) and the Rett syndrome [2]. Accordingly, breath monitoring can be a useful tool for characterising and classifying a wide range of diseases, such as asthma, respiratory arrhythmia, chronic obstructive pulmonary disease (COPD) or cardiac arrest [3].

The conventional measurement techniques for accurately assessing respiratory functions mostly involve contact-based instruments [4]. The polysomnography (PSG) [5] is the de-facto gold standard tool for diagnosis of the respiratory disorders at sleep. However, it is expensive, requires a time-consuming monitoring procedure and generates discomfort for the patients. PSG indeed requires the insertion of a nasal cannula, the application of electrodes to specific body sites and the use of strain gauge and pressure sensors [6] that limits the patient mobility. Other widely used traditional systems [7] are the impedance plethysmography [8], thermistors or flow-meters embedded in a mouthpiece, a mask or a tube. Finally, the stethoscope, which still remains the most common method for diagnosis of breathing problems, is prone to the subjectivity of the physician [9].

Recent years have witnessed the emergence of less invasive wearable monitoring devices and sensorised garments. A coin size acoustic sensor [10] provides a remote real-time access to the sound of the respiratory tract but performs poorly when a patient coughs or sneezes, snores or cries (infants) or is in a noisy surrounding [11]. MEMS (microelectromechanical system) based on three-axis accelerometers have been proposed in [12], [13] to achieve a 3D reconstruction of the movements of the chest wall compartments occurring due to expansion and contraction of the lungs in each respiration act. Although this approach provides an accurate biofeedback regarding breathing frequency and waveform, it however should be used under supervision and in static conditions since body movements may introduce artefacts.

Innovative solutions originate from the significant advances in the Materials science and from the recent evolution of *Skin Electronics* [14] combined with well-assessed Radiofrequency Identification (RFID) technology. The virtuous merging of these disciplines has indeed encouraged the rapid development of a new class of minimally invasive ultra-thin plaster-like devices that can adhere tightly to the soft and curved surface of the skin [15]. Such devices can be wirelessly powered-up and remotely accessed by a reader unit. The absence of batteries, the simple electronics and the reduced amount of conductive elements candidate RFID technology to be one of the most promising solutions for epidermal applications [16].

The idea of using an RFID tag to sense the breath rhythm, by means of the collection of the relative humidity (RH) in the inhalations/exhalations, was recently introduced in [17], [18]. The relative humidity of exhaled breath is higher than the one of the inhaled (ambient) air. Indeed, air in the lungs is almost saturated with water at body temperature of 37°C. During exhalation, the breath goes throughout the cool membrane lining the nose and loses some of its moisture, still maintaining a high water quantity. Finally, the mixture with ambient air at nose level further reduces its moisture content. The RH% of the exhaled breath is hence determined by the velocity/rate and volume of the flux of the air that strictly depend on the human variability and on the health status [19], [20] . Thus, an even qualitative detection of the RH in the surrounding of the nose [19] can provide information about rhythm and intensity of the breath and permits to discriminate different breathing

[1]Manuscript submitted on March 28 2018, and accepted on August 18 2018.
Authors are with the University of Roma Tor Vergata, Via del Politecnico, 1, 00133 Roma (RM). Corresponding author gaetano.marrocco@uniroma2.it

This article has been accepted for publication in a future issue of this journal, but has not been fully edited. Content may change prior to final publication. Citation information: DOI 10.1109/JSEN.2018.2867208, IEEE Sensors Journal

patterns. For this purpose the RFID tag was augmented with a sensor utilising graphene oxide (GO) coating as a sensitive nanomaterial [21] to capture the breath emission.

GO is a graphene derivative, generally obtained by oxidation of graphite in a mixture of strong acid and oxidising agents [22]. Graphene and its derivatives already collected intensive research interest in a wide range of bio-applications thanks to the outstanding physical and chemical properties and, above all, for the intrinsic biocompatibility [23]. Among the several proposed examples, it is indeed worth recalling the lactate detection and the bacterial growth monitoring just inside the mouth [24], [25]. The well known hydrophilic nature of graphene oxide originates from the interactions between the exposed functional oxygen groups and water [26] resulting in good water dispersibility and biocompatibility. In these pioneering experiments, the GO sensor was connected to a general-purpose sensor-oriented RFID board [27] that was applied to a medical face mask. A profile of breath measurement was presented in case of normal respiratory rhythm and apnea. However, the antenna was not optimised for the on-face placement and it was readable up to not more that 30 cm in battery-less mode. A similar approach has been adopted in [28], where a printed graphene sensor has been interfaced to the ADC of a sensor-oriented RFID IC such to wirelessly monitor ammonia. Finally, graphene has been also largely investigated as antenna conductive material in several RFID applications, for example as textile devices [30], analogue sensor [29] and low-cost printing [31].

This work makes a further step toward the real applicability of breath monitoring with GO-based RFID tags by addressing the topic of improving reading range of the tag and discriminating different breath anomalies. By extending the work in [32], it is here described a skin-attachable GO sensor-oriented tag with two-times the read distance of the face mask antenna in [18].

The paper is organised as follows. Section II resumes the nanomaterial-based sensor and its resistance-humidity curve. A flexible antenna, suitable to host such a sensor and to be attached onto the face is introduced in the Section III. Section IV gives details of the fabrication of the epidermal tag prototype and explores the real communication performances when the antenna is directly brought in conformal contact with the cheek of a volunteer. Finally, pivotal results of dynamic characteristics of breathing through an experimental campaign involving ten healthy subjects are presented in Section V, where a simple data processing is introduced to discriminate several breathing patterns (apnea, tachypnea, bradypnea and deep breath).

II. Graphene Oxide-based Sensor

The considered graphene oxide sensor (Fig. 1) is borrowed from [18]. A p-doped silicon (Si) wafer with a 300 nm-thick SiO_2 top layer was used as substrate over which parallel gold electrodes and contacts were photolitographically patterned. 20 nm-thick gold (Au) layer with 2 nm chromium adhesion promotion layer formed two pairs of parallel electrodes separated by 5 μm distance. The larger triangular contact pads were chosen to ease the external connections. During measurements only one pair of electrode was connected to the RFID interface board. The second pair served for redundancy. A 3 µl drop of commercially available graphene oxide solution (2 mg/ml) was drop-cast and left to dry in ambient conditions. While the graphene oxide solution was drying, $10\,V$ peak to peak alternating voltage with $1\,MHz$ frequency generated by function generator was applied between the electrodes. After initial few minutes of drying, a tiny quantity of solution was carefully removed so as to avoid *coffee ring* effect ensuring a uniform deposition during drop evaporation. After complete drying, the substrate was annealed at $195°C$ for 15 minutes on hot plate in dark. Raman characterization confirmed that the film was Graphene oxide. Some degree of reduction was observed but not enough to be termed as a fully reduced-graphene oxide, hence it will be hereafter mentioned simply as Graphene Oxide.

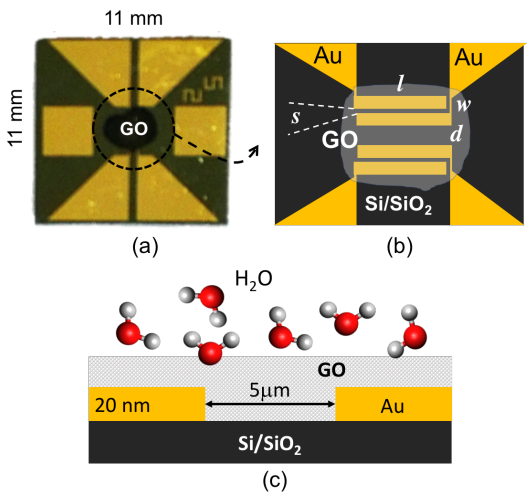

Fig. 1. (a) Prototype of graphene oxide sensor and (b) its top view schematic including a Si/SiO_2 wafer with two pairs of parallel gold (Au) electrodes. Size: l =1000 μm, w=100 μm, s = 5 μm, d = 100 μm; (c) cross section schematic of the device

The calibration curve of the sensor (Fig. 2) is approximately linear with the sensitivity (i.e., the resistance difference generated by 1% change in the relative humidity (RH) level) equal to $S[R] = 60\,\Omega/RH$. The increase in resistance with rising humidity levels originates from the electrostatic adsorption of water molecules over GO surface following the increased interlayer spacing of graphene oxide sheets. In particular, the relative variation of the resistance is about $4\,k\Omega$ within humidity ranging from dry air to $66\%\ RH$. The rise time-constant is 0.9 s.

III. The RFID sensor skin-tag

The tag antenna layout (Fig. 3(a)), to be used in the UHF band $(860 - 960\,MHz)$ [33], comprises a copper trace forming an open loop layout over a PET substrate ($\varepsilon_R = 1.9$, $\sigma = 0.008\ S/m$, and thickness 140 μm). The antenna is

This article has been accepted for publication in a future issue of this journal, but has not been fully edited. Content may change prior to final publication. Citation information: DOI 10.1109/JSEN.2018.2867208, IEEE Sensors Journal

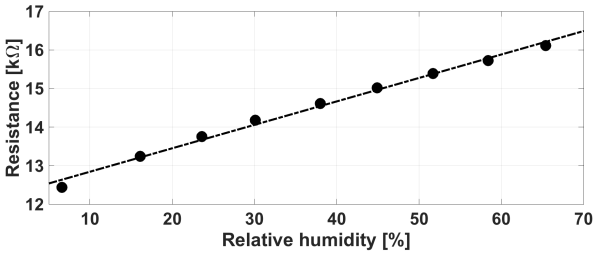

Fig. 2. Calibration curve $R \leftrightarrow RH$ of the GO at room temperature (24 ˚C ± 1 ˚C).

connected to AMS SL900A microchip [34] that is provided with analogue input ports connected to a 10-bit Analog-to-Digital Converter (ADC). External sensors, such as the considered GO, can be directly connected to the SL900A IC sensing ports through the gold electrodes. The variation of the GO resistance due to the sensing activity is hence continuously measured and converted into a digital signal by the internal ADC of the die and then transmitted to the external reader during the conventional RFID interrogation. Since sensor is physically and logically disconnected from the radiation part of the antenna, no impact is expected on its operative frequency or radiation performances.

The size of the antenna meets a possible trade-off between reasonable radiation gain and moderate overall size for application onto the face. The open loop shape of the antenna prevents the input port of the chip to be short-circuited in DC, as required by the data-sheet. The antenna design also includes two pads for the battery connection so that the device will be usable in both fully passive mode (power sensitivity $p_{chip} = -6.9\, dBm$) as well as in battery-assisted passive (BAP) mode ($p_{chip} = -15\, dBm$) so as to significantly improve the read range and also to perform periodic measurements and internally store the data even in absence of the reader (*data-logging* modality).

The antenna response was simulated by means of the Finite-Integration Technique (FIT) modelling in CST Microwave Studio 2017, over a homogeneous standard anthropomorphic model of human head (Fig. 4(a)) with permittivity and conductivity $\epsilon_R = 41.2$ and $\sigma = 0.95\, S/m$.

The performance parameter to be maximised in this configuration was the power transfer coefficient for the tag's antennas-microchip interface, $\tau = \frac{4R_{chip}R_A}{|Z_{chip}+Z_A|^2} \leq 1$, where $Z_A = R_A + jX_A$ is the input impedance of the tag's antenna and $Z_{chip} = 123 - j303\ \Omega$ is the RF equivalent impedance of the microchip at 915 MHz for harvesting mode. For this purpose, the antenna meanders (a and b) were hence properly sized in order to match the resistance of the chip. The antenna reactance was adjusted by the use of a lumped tuning inductor L placed between the microchip and the antenna. The numerical simulation included a real inductor model [35] (Fig. 3(b)) with the purpose to properly account for the frequency detuning due to possible self-resonance and parasitic effects.

Fig. 4(b) shows the simulated power transfer coefficient of

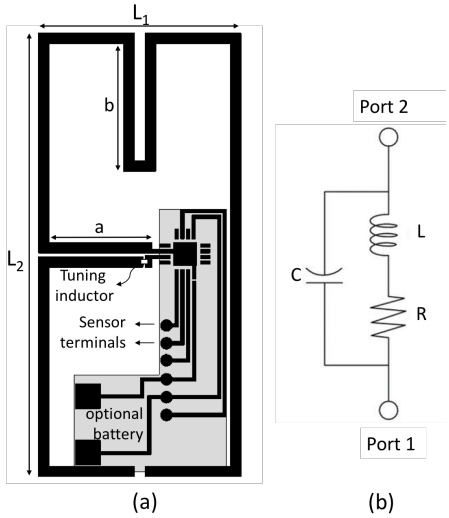

Fig. 3. (a) Open loop antenna layout. Size [mm]: $L_1 = 28.5$, $L_2 = 62.5$, $a = 14.5$ and $b = 18$. (b) Scheme of the real tuning inductor.

the tag for different values of inductance. The peak of the power transfer coefficient is quite stable ($0.9 < \tau < 1$) for $L = \{47,\ 51,\ 56,\ 62\}\ nH$. Therefore, the antenna response may be easily tuned in the European (866 - 869 MHz), in the North American (902 - 928 MHz) or Japanese (952 - 956 MHz) RFID frequency bands *fr* by simply selecting a proper inductor.

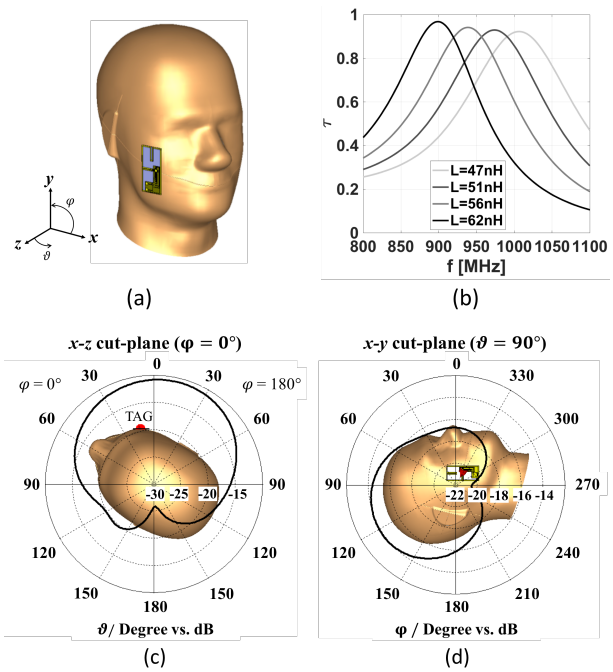

Fig. 4. (a) Skin antenna over a homogeneous numerical head phantom. (b) Simulated power transfer coefficient τ for some values of the lumped tuning inductor. (c) Gain polar plot at 915 MHz onto a transverse plane and (d) onto a sagittal plane (max gain = -11 dB).

The gain pattern is represented in Fig. 4(c-d) on the

This article has been accepted for publication in a future issue of this journal, but has not been fully edited. Content may change prior to final publication. Citation information: DOI 10.1109/JSEN.2018.2867208, IEEE Sensors Journal

transverse and sagittal planes. The gain peak of -11 dBi at 915 MHz is comparable with those of other reported epidermal antennas which span between -20 and -10 dBi [36]. Moreover, the *realized gain* $G_\tau = G \cdot \tau$ is more than -15 dBi within an angle of about 120° on the transverse plane and practically constant with respect to the peak value within an angle of 60°. Accordingly, the communication link between a fixed antenna and the face can be considered tolerant to moderate tilt and rotations of the head especially if a circular-polarized interrogating antenna is used instead of a linear one. It is finally worth noticing that the gain of the proposed antenna is 6 dB better than the face mask tag configuration described in [18] (max realized gain: -17 dBi) so that a two-times read distance is expected with respect to the previous arrangement.

A. Safety issue

As the proposed measurement device involves the exposure of the head to the interrogating electromagnetic field, it is worth evaluating the localized Specific Absorption Rate ($SAR = \frac{1}{2\rho}\sigma\,|E|^2$, ρ and σ being the mass density and the conductivity of the head phantom, respectively) averaged over 10 g of tissue when an interrogating antenna is placed in the near proximity of the face (at a distance of 15 cm). The considered antenna (to be later on applied for measurements) is a broadband linear-polarized stacked planar inverted-F (SPIFA) over closed-cell PVC foam-board with external size $13cm \times 20cm$ and maximum gain of 5 dBi along the broadside direction.

The numerically estimated SAR corresponding to 1 W reader's output power is reported in Fig. 5. The peak value is of the order of $\sim 10^{-6}$ W/kg), i.e much below the limit 2 W/kg (averaged over 10 g of tissues) imposed by regulation for the head [37]. Accordingly, the UHF interrogation of the integrated system can be considered completely compliant with SAR exposure limits.

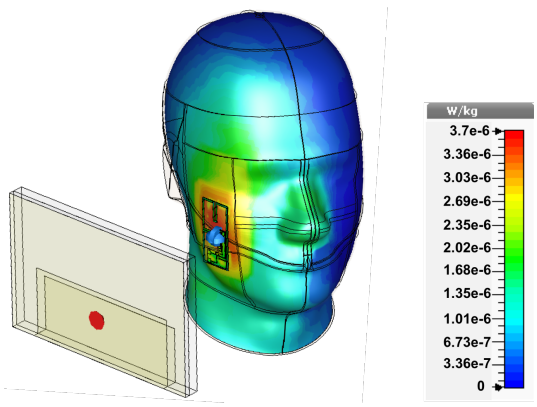

Fig. 5. SAR distribution produced in the face by the reader's antenna placed at 15 cm from the skin-mounted antenna and fed by 1 W input power.

IV. Prototype and Characterization

A prototype of the antenna (Fig. 6) was fabricated by carving a flexible adhesive-backed copper foil (35 μm thickness) attached on a 140 μm thin PET (polyethylene terephthalate) film ($\epsilon_R = 1.9$ and $\sigma = 0.008\ S/m$) by means of a two-axis digital-controlled cutting plotter. Both the traces for the sensor interconnections and the battery were manufactured by etching a flexible 50 μm-thick Kapton substrate. The carved copper and the flexible PCB were then integrated together by means of a biocompatible 20 μm-thin polyurethane adhesive film (Rollflex film from Master-AID) here used as a substrate. The graphene oxide sensor, placed on a FR4 square substrate, as holder, was then loosely connected to two pins of the microchip by means of thin insulated wires for an independent placement with respect to the tag transponder.

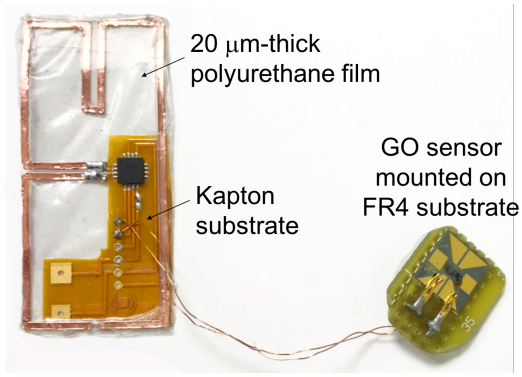

Fig. 6. Prototype of the passive tag (tuning inductor L = 56 nH) connecting the graphene oxide sensor.

The communication performance of the prototype was characterized through the measurement of the realized gain G_τ when it was attached onto a tank filled with a liquid phantom (a mixture of water, sugar and salt with $\epsilon_R = 41.2$, $\sigma = 0.95\,S/m$) emulating the human tissue. In a second measurement the tag was then directly placed onto the face of a volunteer. The interrogating measurement setup comprised a typical long-range UHF fixed reader (*ThingMagic* M5 ASIC) connected to SPIFA antenna introduced above.

Fig. 7 shows the measured realized gain (retrieved by the turn-on procedure [38]) compared with the numerical simulation for corroboration. Despite of a frequency shift due to the combination of an un-perfect manual fabrication of the antenna with the only rough correspondence between the materials of the numerical phantom and the real face of the volunteer (nor the liquid phantom), the simulated data anyway lays in between the two series of experimental data. Overall, the average error between simulations and on-the face measurements is roughly less that 1dB and 2dB in the European and US/Japan bands, respectively.

The measured antenna response is quite broadband and almost flat because of the high loss of the human head. The measurement over the bottle underestimates the performance of about 2-3 dB, thus this phantom could be considered conservative for repeatable experimental verification of the tag performance. By assuming the reader's antenna is fed by 1 W, the maximum read distance of the device in passive mode, i.e. with no battery onboard, can be estimated as 60 cm (40 cm)

This article has been accepted for publication in a future issue of this journal, but has not been fully edited. Content may change prior to final publication. Citation information: DOI 10.1109/JSEN.2018.2867208, IEEE Sensors Journal

in case of linear- (circular)-polarized reader, i.e. twice the the distance found for the face-mask antenna in [18].

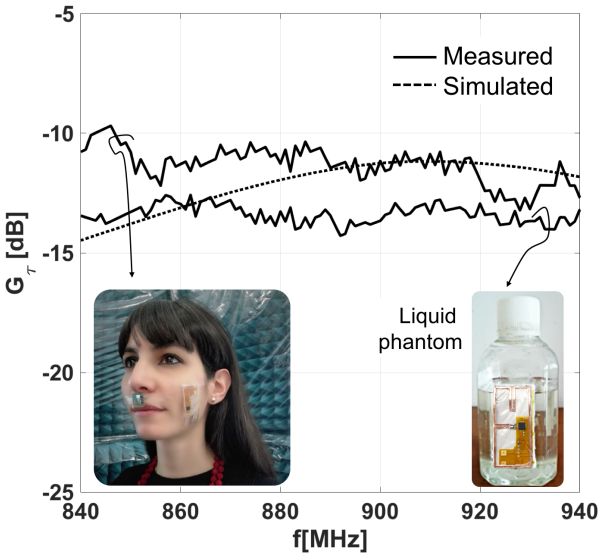

Fig. 7. Measured and simulated realized gain G_τ of the tag attached directly onto a homogeneous liquid phantom and onto volunteer's cheek.

V. Breath patterns detection: experimentation with volunteers

The potentialities of the proposed epidermal device are now investigated by means of a realistic experimental session involving the supervised monitoring of breathing.

A. Test set-up

The graphene oxide-based sensor was evaluated on a group of ten healthy young volunteers, 3 males and 7 females with age ranging from 25 to 33 years. The volunteers engaged in the experiments were properly informed about the purpose of the study and signed an informed consent before participation. The volunteers were asked to perform for about 8 minutes, in sitting position, five different breathing patterns: a normal breathing, a deep breathing so that the air coming in through the nose fully fills their lungs and the lower belly rises, as well as some patterns that were derived from various types of respiratory disorders such as apneas, tachypnea, i.e. a rapid and shallow respiration, and bradypnea, which is an abnormally slow breathing condition.

The battery-less tag was attached directly on the cheek of the volunteers by means of medical adhesive tape. The tag antenna was aligned with the reader antenna (same height and polarization match) placed at $40\ cm$ distance from the subject, while the graphene oxide resistive sensor probe was placed in close contact with the nose.

All volunteers were instructed to breath at a metronome rate according to a timed beeping sound programmed at a chosen frequency as in Tab. I. Apnea was emulating by requesting the participants to pause breathing for at least 60 sec. The total duration of apnea event depends on the peculiar capability of each volunteer to interrupt the air inhalation for a time window marked by a timer. Moreover, we assigned a 2 min-rest interval after each pattern.

TABLE I
Respirations per minute (rpm) of breath patterns under test.

Normal	Deep	Tachypnea	Bradypnea	Apnea
12 - 20	12 - 20	> 25	< 12	0

B. Measured profiles

Figure 8.(a) shows an example of the measured profile of resistance of graphene oxide following the exposure to humidity emitted during some breathing patterns[2]. The changes in resistance for each breath cycle are clearly detectable in comparison with the signal fluctuation occurring, in particular, during the temporary suspension of breathing (apnea condition). During the exhalation, human breath is strongly humidified, and therefore the amount of water on the surface of the graphene oxide coating increases, and in turn its resistance. Instead, during the breathing in, the amount of water absorbed by the graphene oxide electrode is reduced since the relative humidity of the surrounding environment is almost always lower than the exhaled air. The estimated maximum average dynamic range of the normal breathing signal ($80\ \Omega$) is indeed much higher than the standard deviation value of the noise level ($6.2\ \Omega$). The early transient is affected by a significant drift, probably due to the large difference in drying and humidifying cycles during breathing. The drift vanishes in a few minutes when a chemical equilibrium is reached.

C. Data Processing

The sensor output is processed in order to extract two features for each respiration pattern, e.g. the dynamic range ΔR of the GO resistance and the respiratory rate, which is a recognized key parameter for the diagnosis and monitoring of a wide range of breathing disorders and useful broader indicator of a patient's condition. For this purpose, the drift is preliminary removed by a high-pass filtering (first-order derivative) still preserving the difference between the breathing modes (Fig. 8(b)). After that, the breathing trace of each volunteer is decomposed into time-frames, each corresponding to a different breathing pattern. The dynamic range ΔR is hence evaluated as the average difference between maximum and minimum resistances corresponding to consecutive inhalation-exhalation acts within each time frame. The Fast Fourier Transform (FFT) is finally applied to derive the respiratory rate corresponding to the peak value. As an example, the spectrum of the trace in Fig. 8(b) is shown in Fig. 9. Three distinct peaks are visible: the first one at $0.13\ Hz$ (approximately 8 rpm) corresponds to the breathing frequency in bradypnea condition,

[2]A video demonstrating the real-time detection of different respiratory patterns is available online at the following link https://www.youtube.com/watch?v=cEbpfayG38c.

This article has been accepted for publication in a future issue of this journal, but has not been fully edited. Content may change prior to final publication. Citation information: DOI 10.1109/JSEN.2018.2867208, IEEE Sensors Journal

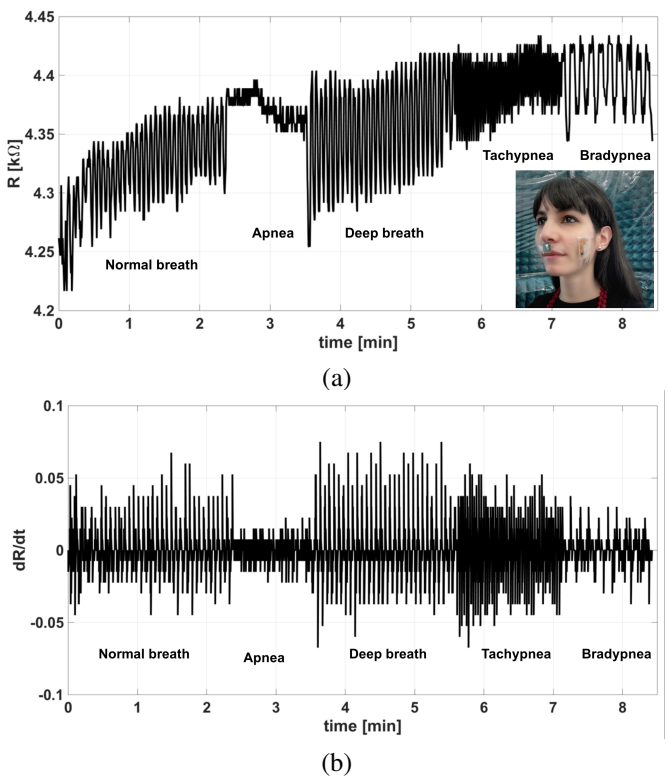

Fig. 8. (a) Respiratory patterns of a subject recorded when the antenna, embedding the graphene oxide sensor, is directly stuck on face. (b) High pass filtering of the acquired breathing signal during the exercise.

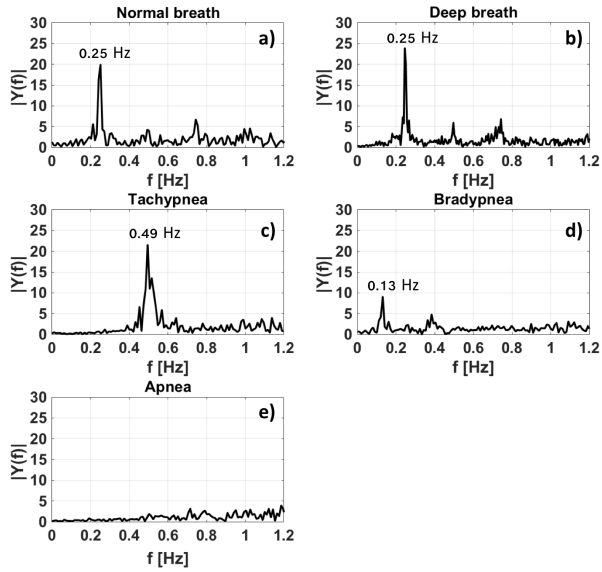

Fig. 9. Frequency spectra of the breathing signature computed in the five time windows in Fig. 8.(b) corresponding to *a*) normal breathing, *b*) deep breathing, *c*) tachypnea, *d*) bradypnea and *e*) apnea.

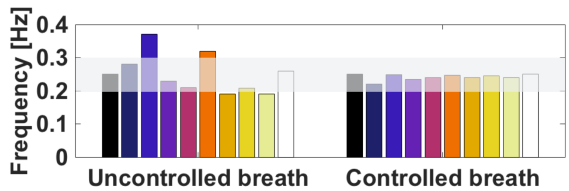

Fig. 10. Both uncontrolled and controlled free breathing rate of the ten participants to the test.

the second sharp peak at $0.25\ Hz$ (15 rpm) corresponds to the normal or deep breathing frequency, while the third peak at about $0.5\ Hz$ (30 rpm) corresponds to a more rapid breathing which is typical in subjects affected by tachypnea. The spectral content of each breath pattern spreads over the entire frequency band due to the noise signal level collected by the device during the prolonged interruption of breathing (apnea event).

D. Aggregated analysis

A preliminary analysis concerns the normal breath. Fig 10 shows the respiratory rate of all the volunteers in case of spontaneous inhalation-exhalation as well as in controlled condition, lead by a metronome. While the rate of free breath of all the ten volunteers fall in the range of 12 - 22 rpm (0.2 - 0.37 Hz), the controlled response is constrained in a the narrower range of 12-15 rpm (0.2-0.25 Hz) and hence the experiments of all the volunteers can be considered repeatable, and hence comparable.

By application of the above introduced data processing to all the breathing traces, the multi-parameter butterfly chart in Fig. 11(a) is obtained. The diagram shows both the distribution of the dynamic range of the graphene oxide resistance (ΔR) between inhalations and exhalations for each volunteer and the distribution of breathing rates corresponding to the five different breathing patterns. Frequencies of each respiratory pattern are rather uniform over the set of volunteers thanks to the metronome control that induces a regular inhalation/exhalation, as discussed above. Distributions of dynamic ranges of the resistances are instead much less uniform thus indicating a relevant subjectivity. Some outliers are visible for the bradypnea, deep breath, and tachypnea probably due to an over-hydration status of the sensor caused by an excessive amount of water remaining trapped on the graphene oxide during the previous exhalation in case of some of the volunteers.

It is worth noting that different breath patterns produce similar average resistances (normal breath and tachypnea), while other families of respirations are characterized by a same frequency (normal and deep breathing). Accordingly, a single feature is not enough to achieve a correct discrimination of the considered breath patterns and both resistance and frequency are required.

In detail, the scatter plot of Fig.11(b) shows a clear tendency to separate the four groups. Interestingly, most of the overlaps occurs between healthy breaths (normal and deep) while anomalous behaviours are clearly distinct. In particular, tachypnea, bradypnea and apnea are sharply discriminated by means of the only frequency analysis. Normal and deep respiratory rhythms obviously share the same frequency but can be nevertheless recognized throught the analysis of resis-

This article has been accepted for publication in a future issue of this journal, but has not been fully edited. Content may change prior to final publication. Citation information: DOI 10.1109/JSEN.2018.2867208, IEEE Sensors Journal

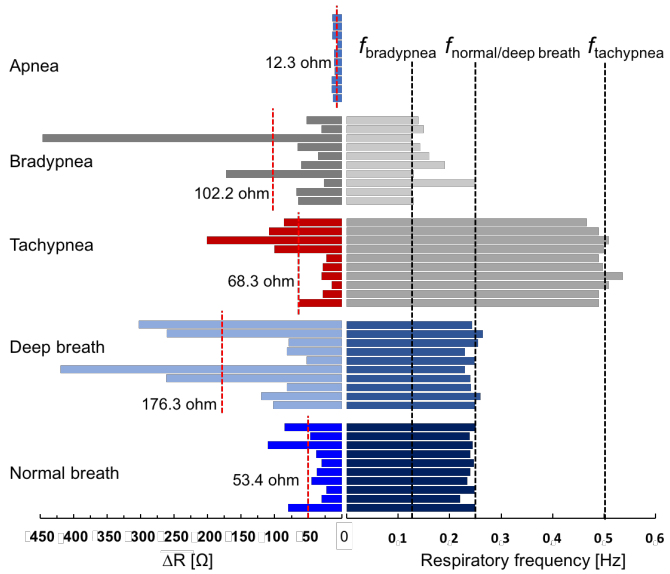

(a)

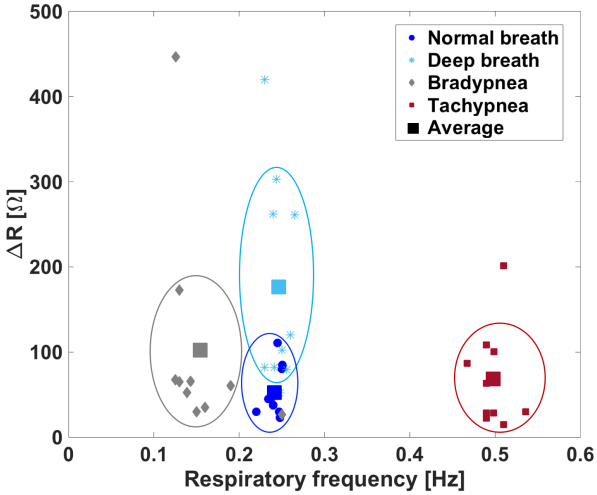

(b)

Fig. 11. (a) Butterfly distributions of both dynamic ranges and frequencies; dotted lines represent the average values of the bars among the ten volunteers, for each breathing pattern. (b) Data Clusterization (apnea not reported as it lacks a peak resonance).

tances whose average values are rather different. Deep breath is indeed wetter than the normal breath. Overall, there is an apparent in-correlation between the two considered features (frequency and resistance). The clustering of data in Fig.11(b) can be quantitatively expressed by the accuracy of a classification model. For the scope, a Decision Tree algorithm [39] complemented by a 10-fold cross-validation has been applied to the data in Fig. 11. The accuracy of the classifier is about 88% (confusion matrix in Tab. II).

TABLE II
CONFUSION MATRIX OF THE CROSS-VALIDATED DECISION TREE CLASSIFIER

True Class \ Predicted Class	*Apnea*	*Brady*	*Deep*	*Normal*	*Tachy*
Apnea	100 %	0	0	0	0
Brady	0	80 %	0	20 %	0
Deep	0	0	90 %	10 %	0
Normal	0	0	30 %	70 %	0
Tachy	0	0	0	0	100 %

VI. DISCUSSIONS AND CONCLUSIONS

We have presented a wireless wearable RFID device, combining a flexible antenna and a GO sensitive coating. The performance of the proposed radio-sensor is compared in Table III with state of the art devices for breath monitoring, concerning in particular the nonediscretization levels[3] of the measured breathing waveform for an adult at rest that breaths spontaneously. The number of discrete levels of the proposed sensor is 19, i.e. less than other systems due to the limited resolution of the particular RFID sensor-oriented chip (including just a 10 bits ADC) used in the prototype. The resolution is however expected to improve by new generation of sensor-oriented RFID chips with a better ADC. Nevertheless, this even modest resolution permitted to discriminate several breath patterns.

Unlike other solutions, the proposed device enables a direct measurement of the human breath unlike those other systems that instead measure quantities indirectly related to breathing (e.g., torso expansion and contraction). The GO-based RFID tag looks moreover more comfortable than thermal airflow sensors, like thermistors or accurate flowmeters like pneumotachograph that have to be embedded in a nasal cannula and mouthpieces or on a mask for the measurement, and make hence difficult the prolonged monitoring of respiration.

The measurement configuration that was experimented so far, included a sensor probe spaced apart from the RFID tag. A more effective implementation would instead benefit of an integrated and unique device. Further research efforts will be therefore oriented to reshape the tag layout and to deliver the nanomaterial directly within the tag surface so that the device could be applied like an anti-snoring nasal plaster by using a rubber stamp or the usual inkjet printing technique. Additionally, the biological and chemical functionalization of the nanomaterial could enable a multi-parametric identification of the volatile compounds in the breath which may help to identify and manage patients at risk and thereby reducing the occurrence of serious adverse events. A clinical experimental analysis is required to statistically validate the robustness and the detection features of the radio sensor in real conditions.

The very critical issue with the proposed system, and with epidermal electronic in general, is the modest read-distance that could be partly extended (up to three times) by providing

[3]The discretization levels of the measured breath signal is defined as $levels = {}^{DR}/_{\delta_R}$ where DR is the dynamic range of the data measured and δ_R is the intrinsic resolution of the acquisition system.

This article has been accepted for publication in a future issue of this journal, but has not been fully edited. Content may change prior to final publication. Citation information: DOI 10.1109/JSEN.2018.2867208, IEEE Sensors Journal

TABLE III
COMPARISON OF RESPIRATION MONITORING METHODS.

Sensor type	Detected Variable	Output signal	Volume & Weight	Skin adhesion system	Connection Type	Levels
Resistive sensor (This work)	% RH content in the airflow	Resistance [Ω]	6.2 x 2.8 x 0.07 cm^3 (antenna) 2.4 gr (antenna + sensor)	Biocompatible adhesive	Wireless (840 - 960 MHz)	19* (10-bit)
Strain gauge transducer [40]	Changes in thoracic or abdominal circumference	Length [cm]	6.6 cm x 4 cm x cm 1.5 18 gr	Nylon strap Velcro®	Wired	2450 (16-bit)
Thermistor [41]	Airflow temperature	Voltage [mV]	60 cm key connector 200 cm DIN connector	Nasal cannula	Wired	n. a.
Motion sensor [12]	Three axis-acceleration	Acceleration m/s^2	2.2 cm x 1.5 cm 1.5 gr	Elastic strap	Bluetooth (2.4 to 2.84 GHz)	1536 (12 -bit)
Respiration transducer record [42]	Changes in thoracic or abdominal circumference	Voltage [V]	6 cm x 4 cm x 2 cm 54 gr	Electrode & gel + belt/t-shirt	Wireless (2.4 GHz)	154 (12-bit)
Bioharness - Zephyr sensor [43]	Breaths per minute	bpm	2.8 cm (diameter) x 0.7 cm x 0.5 cm (strap width) 68 gr	Elastic strap	Bluetooth (2.4 to 2.84 GHz)	696 (12-bit)
Electrical bioimpedance amplifier [44]	Thorax resistance	Resistance [Ω]	4 cm x 11 cm x 19 cm 380 gr	Electrode & gel	Wired	75 (16-bit)

* The number of levels may vary up to 59 and 1194 in the case of 12 and 16 bit-ADC resolution, respectively.

the sensor with a battery thus forcing the chip to work in BAP mode. The read performance is however expected to improve in the near future by means of forthcoming new generations of sensing-oriented chips. Anyway, the current achievable read distances, even if modest, could enable useful applications such as *i*) to get breath information (a few respiration periods) when the user crosses a door (for instance inside his home) and *ii*) to continuously monitor a patient in real-time provided that he is steady, fixed in a reference position, or alternatively he is sleeping with multiple antennas properly located around his bed.

ACKNOWLEDGEMENT

Work partly supported by the project SECOND SKIN funded by Lazio Innova "Gruppi di Ricerca".

REFERENCES

[1] K. Barrett, S. Barman, S. Boitano, and H. L. Brooks, "Ganong's Review of Medical Physiology," New York: McGraw-Hill Medical, 23rd Ed., 2009.

[2] T. W. Huang, M. Y. Kochukov, C. S. Ward, J. Merritt, K. Thomas, T. Nguyen, B. R. Arenkiel, J. L. Neul, "Progressive Changes in a Distributed Neural Circuit Underlie Breathing Abnormalities in Mice Lacking MeCP2," *The Journal of Neuroscience*, vol. 36, no. 20, pp. 5572 - 5586, May 2016.

[3] N. Rubio, R. A. Parker, E. M. Drost, H. Pinnock, C. J. Weir, J. Hanley, L. C. Mantoani, W. MacNee, B. McKinstry, and R. A. Rabinovich, "Home monitoring of breathing rate in people with chronic obstructive pulmonary disease: observational study of feasibility, acceptability, and change after exacerbation," *International Journal of Chronic Obstructive Pulmonary Disease*, vol. 12, pp. 1221-1231, 2017.

[4] A. Aliverti, "Wearable Technology: Role in Respiratory Health and Disease," *Breath*e, vol. 13, no. 2, pp. e27 - e36, June 2017.

[5] Z. Zaiwalla, and R. Killick, "Polysomnography and other investigations for sleep disorders," *Oxford Textbook of Clinical Neurophysiology* ,187, 2017.

[6] Y. Khan, A. E. Ostfeld, C. M. Lochner, A. Pierre, A. C. Arias, "Monitoring of Vital Signs with Flexible and Wearable Medical Devices," *Advanced Materials*, vol. 28, pp. 4373 - 4395, 2016.

[7] Firat Güder, Alar Ainla, Julia Redston, Bobak Mosadegh, Ana Glavan, T. J. Martin, and George M. Whitesides, "Paper-Based Electrical Respiration Sensor", *Angewandte Chemie International Edition*, Vol. 55, no. 19, pp. 5727 – 5732, 2016.

[8] M. C. Lee, A. C. Klassen, L. M. Heaney, J. A. Resch, "Respiratory rate and pattern disturbances in acute brain stem infarction," *Stroke*, vol. 7, no. 4, pp. 382-385, 1976.

[9] N. Gavriely, "Breath Sounds Methodology," Boca Raton, FL, USA, *CRC Press*, 1995.

[10] Acupebble. [Online]. Available: http://www.acupebble.com.

[11] F. Q Al-Khalidi, R. Saatchi, D. Burke, H. E. Elphick, S. Tan, "Respiration Rate Monitoring Methods: A Review," *Pediatric Pulmonology, Wiley*, vol. 46, no. 6, pp. 523 - 529, 2011.

[12] A. Roshan Fekr, M. Janidarmian, K. Radecka, and Z. Zilic, "Respiration Disorders Classification With Informative Features for m-Health Applications," *IEEE Journal of Biomedical and Health Informatics*, Vol. 20, no. 3, May 2016.

[13] M. Janidarmian, A. R. Fekr, K. Radecka, and Z. Zilic, "Multi-Objective Hierarchical Classification Using Wearable Sensors in a Health Application," *IEEE Sensors Journal*, vol. 17, no. 5, pp. 1421 - 1433, March 2017.

[14] J. A. Rogers, R. Ghaffari, D.-H. Kim, "Stretchable Bioelectronics for Medical Devices and Systems," *Springer*, 2016.

[15] H. Jin, Y. S. Abu-Raya, and H. Haick, "Advanced Materials for Health Monitoring with Skin-Based Wearable Devices," *Advanced Healthcare Material*, 2017.

[16] Amendola, S. , Occhiuzzi, C. and Marrocco, G. (2016). More than Wearable: Epidermal Antennas for Tracking and Sensing. In Electromagnetics of Body Area Networks (eds D. H. Werner and Z. H. Jiang). doi:10.1002/9781119082910.ch9

[17] M. C. Caccami, M.Y. S. Mulla, C. Di Natale, G. Marrocco, "Wireless Monitoring of Breath by means of a Graphene Oxide-based Radiofrequency Identification Wearable Sensor," *11th European Conference on Antennas and Propagation*, 19 - 24 March 2017, Paris, France.

[18] M. C. Caccami, M. Y. S. Mulla, C. Di Natale, G. Marrocco, "Graphene oxide-based radiofrequency identification wearable sensor for breath monitoring", *Trans. of IET Microwaves, Antennas & Propagation*, vol.12, no.4, pp 467-471, Jan. 2018.

[19] Umesha Mogera, A. Abhay Sagade, Subi J. George, George & Giridhar, U. Kulkarni, "Ultrafast response humidity sensor using supramolecular nanofibre and its application in monitoring breath humidity and flow", *Scientific Reports,* vol. 4, Article number: 4103, 2014.

[20] J. Mathew, Y. Semenova, and G. Farrell, "A miniature optical breathing sensor," *Biomed Opt Express.*, Dec. 2012, vol. 3, no. 12, pp. 3325–3331. doi:10.1364/BOE.3.003325

[21] M. Zhang, R. R. Naik, and L. Dai, "Carbon Nanomaterials for Biomedical Applications," vol. 5, *Springer Series in Biomaterials Science and Engineering,* 2016.

[22] S. S. Nanda, G. C. Papaefthymiou, and D. K. Yi, "Functionalization of Graphene Oxide and its Biomedical Applications," *Critical Reviews In Solid State And Materials Sciences*, Vol. 40, no. 5, 2015.

[23] Liu, Z.M., Shen, Z.H., Zhang, L.: 'Biomedical applications of graphene', Theranostics, 2012, 3, (2), pp. 283–294

[24] P. Labroo, Y. Cui, "Flexible graphene bio-nanosensor for lactate," *Biosensors and Bioelectronics*, 41, pp 852 - 856, 2013.

[25] M. S. Mannoor, H. Tao, J.D. Clayton, A. Sengupta, D.L. Kaplan, R.R. Naik, N. Verma, F. G. Omenetto, and M. C. McAlpine, "Graphene-based wireless bacteria detection on tooth enamel," *Nature Communications* 3, no. 763, 2012.

[26] S. Borini, R. White, D. Wei, M. Astley, S. Haque, E. Spigone, N. Harris, J. Kivioja, and T. Ryhänen, "Ultrafast Graphene Oxide Humidity Sensors," *ACS Nano*, vol. 7, no. 12, pp. 11166 - 11173, 2013.

[27] C. Occhiuzzi ; S. Amendola ; S. Manzari ; S. Caizzone ; G. Marrocco, "Configurable radiofrequency identification sensing breadboard for industrial Internet of Things, *Electronics Letters* , vol. 53, no. 3, pp. 129 - 130, 2017.

[28] T. Le et al., "A novel graphene-based inkjet-printed WISP-enabled wireless gas sensor," 2012 42nd European Microwave Conference, Amsterdam, 2012, pp. 412-415. doi: 10.23919/EuMC.2012.6459158

[29] Leng, T., Huang, X., Chang, K., et al.: 'Graphene nanoflakes printed flexible meandered-line dipole antenna on paper substrate for low-cost RFID and sensing applications', IEEE Antennas Wirel. Propag. Lett., 2016, 15, pp. 1565–1568

[30] Akbari, M., Virkki, J., Sydänheimo, L., et al.: 'Toward graphene-based passive UHF RFID textile tags: A reliability study', IEEE Trans. Device Mater. Reliab., 2016, 16, (3), pp. 429–431

[31] P. Kopyt et al., "Graphene-Based Dipole Antenna for a UHF RFID Tag," in IEEE Transactions on Antennas and Propagation, vol. 64, no. 7, pp. 2862-2868, July 2016. doi: 10.1109/TAP.2016.2565696

[32] M. C. Caccami, C. Miozzi, M. Y. S. Mulla, C. Di Natale, and G. Marrocco, "An Epidermal Graphene Oxide-based RFID Sensor for the Wireless Analysis of Human Breath," *8th Annual IEEE International Conference on RFID Technology and Applications*, 20 - 22 September 2017, Warsaw, Poland.

[33] S. Amendola, G. Bovesecchi, A. Palombi, P. Coppa, and G. Marrocco, *"*Design, Calibration and Experimentation of an Epidermal RFID Sensor for Remote Temperature Monitoring*," IEEE Sensors Journal*, vol. 16, no. 19, pp. 7250-7257, Oct. 2016.

[34] AMS SL900A Tag Chip Datasheet. Online Available at https://ams.com/ger/content/ download/755603/1912935/file/SL900A_Datasheet_EN_v5.pdf.

[35] Murata. [Online]. Available: http://www.murata.com.

[36] S. Amendola, G. Marrocco, "Optimal Performance of Epidermal Antennas for UHF Radiofrequency Identification and Sensing," *IEEE Transactions on Antennas and Propagation*, vol. 65, no. 2, pp. 473-481, Feb. 2017.

[37] European Parliament, "Directive on the minimum health and safety requirements regarding the exposure of workers to the risks arising from physical agents (electromagnetic fields), 2013/35/EU.

[38] P. V. Nikitin and K. V. S. Rao, "Theory and measurement of backscattering from RFID tags," *IEEE Antennas Propagation Magazine*, vol. 48, no. 6, pp. 212 - 218, Dec. 2006.

[39] M. Oded Z., R. Lior, "Data Mining With Decision Trees: Theory And Applications" (2nd Edition), in *Series In Machine Perception And Artificial Intelligence*, World Scientific, vol. 81, 2014.

[40] Biopac System, Inc. TSD201 Transducer Datasheet. [Online]. Available: https://www.biopac.com/wp-content/uploads/TSD201.pdf.

[41] SleepSense Thermal Flow Sensors User Manual. [Online]. Available: https://cdn.shopify.com/s/files/1/1046/1086/files/SleepSense-Thermal-Flow-Sensors-User-Manual.pdf.

[42] Biopac System, Inc. BIONOMADIX Product sheet. [Online]. Available: https://www.biopac.com/wp-content/uploads/BioNomadix-Series.pdf.

[43] Zephyr™ BioHarness 3.0 User Manual, [Online]. Available: https://www.zephyranywhere.com/media/download/bioharness3-user-manual.pdf.

[44] Biopac System, Inc. EBI100C Electrical Bioimpedance Amplifier. [Online]. Available: https://www.biopac.com/wp-content/uploads/EBI100C.pdf.